STRESSES CAUSED BY AN IN-PLANE LINE LOAD USED TO ROTATE A THIN-WALLED SPHERICAL SATELLITE

by W. Jefferson Stroud and Nancy P. Sykes

Langley Research Center
Langley Station, Hampton, Va.

NATIONAL AERONAUTICS AND SPACE ADMINISTRATION • WASHINGTON, D. C. • APRIL 1968

STRESSES CAUSED BY AN IN-PLANE LINE LOAD USED TO ROTATE A THIN-WALLED SPHERICAL SATELLITE

By W. Jefferson Stroud and Nancy P. Sykes

Langley Research Center
Langley Station, Hampton, Va.

NATIONAL AERONAUTICS AND SPACE ADMINISTRATION

For sale by the Clearinghouse for Federal Scientific and Technical Information
Springfield, Virginia 22151 – CFSTI price $3.00

STRESSES CAUSED BY AN IN-PLANE LINE LOAD USED TO ROTATE A THIN-WALLED SPHERICAL SATELLITE

By W. Jefferson Stroud and Nancy P. Sykes
Langley Research Center

SUMMARY

The stress resultants and deformations which are brought about by a sinusoidal in-plane line load acting along a great circle of a spherical satellite of the Echo type are calculated and are presented in contour plots and in tabular form. The line load is applied in order to rotate the thin-walled spherical satellite for station-keeping purposes. The line load is induced by the interaction of a current-carrying wire with the geomagnetic field. Linear membrane theory and numerical methods are used in the analysis.

INTRODUCTION

One method for obtaining orbit position control of large, inflatable, spherical, passive communications satellites of the Echo type is to utilize forces caused by solar photon flux on the satellite's surface. These forces are dependent upon the reflectance, absorptance, and emittance properties of the surface of the satellite. The satellite's surface could be divided into regions having different values of these properties. By adjusting the orientation of the satellite so that a desired surface faces the sun, the forces caused by solar radiation pressure could be modulated and used to control the orbit of, or "station keep," the satellite. To obtain the desired orientation the satellite could be rotated by torques resulting from the interaction of the earth's magnetic field with electric current carried by wires mounted on the surface of the satellite. A discussion of this type of station-keeping system is contained in reference 1.

In the present paper an analysis is made of the stresses in and deformations of a thin-walled spherical shell with a single current-carrying wire mounted on a great circle of the sphere and interacting with the geomagnetic field. The interaction causes both in-plane and radial loads on the sphere. Only the effects of the in-plane component of the applied line load and the resulting inertia load caused by angular acceleration are considered. Linear membrane theory and numerical methods are used in the analysis. Results are given as contour plots and as a table of stresses and displacements over the surface of the spherical shell.

SYMBOLS

The physical quantities used in this paper are given both in the U.S. Customary System of Units and in the International System of Units (SI) (ref. 2). Appendix A presents factors relating these two systems of units.

$A = IB \cos \beta$

a_1 constant associated with homogeneous solution of differential equation for $N_{\theta,0}$ (see eq. (B7))

B flux density of geomagnetic field (see eq. (1))

b direction of geomagnetic field (see figs. 1 and 2)

D bending stiffness

E Young's modulus

$d\vec{F}$ differential force on wire

dF_i in-plane component of $d\vec{F}$

dF_r out-of-plane (radial) component of $d\vec{F}$

I current in wire (see eq. (1))

$\hat{I}$ area moment of inertia of cross section of sphere (see eqs. (B13) and (B16))

I_ρ polar mass moment of inertia of sphere (see eq. (7))

K extensional stiffness

$d\ell$ differential length along wire

N_n principal stress, $\sqrt{N_\theta^2 + N_{\theta\phi}^2}$ for problem herein

$N_\theta, N_\phi, N_{\theta\phi}$ in-plane stress resultants

$N_{\theta,0}, N_{\theta,1}, \ldots, N_{\theta,i}, \ldots$ functions of θ which appear as coefficients in power series expansion for N_θ (see eq. (B4))

$N_{\theta\phi,0}, N_{\theta\phi,1}, \ldots, N_{\theta\phi,i}, \ldots$ functions of θ which appear as coefficients in power series expansion for $N_{\theta\phi}$ (see eq. (C18))

P_θ, P_ϕ, P_r loading per unit area in θ, ϕ, and radial directions, respectively

r radius of sphere

t wall thickness of sphere

u,v,w displacements in θ, ϕ, and radial directions, respectively

$\bar{u} = \frac{u}{\sin \phi}$

V shear load (see eq. (B11))

$v_0, v_1, \ldots, v_i, \ldots$ functions of θ which appear as coefficients in power series expansion for v (see eq. (C19))

X,Y,Z axis system (see figs. 1 and 2)

α angular acceleration

β angle between plane of wire and earth's magnetic field (see figs. 1 and 2)

$\epsilon_\theta, \epsilon_\phi, \gamma_{\theta\phi}$ in-plane strains

θ, ϕ circumferential and meridional coordinates of the spherical coordinate system (see fig. 2)

$\Delta\theta, \Delta\phi$ increments in θ and ϕ directions, respectively, used in the numerical calculation of N_θ

μ Poisson's ratio

ξ dummy variable of integration (see eq. (B14))

ρ mass per unit area of sphere

ω relaxation factor

LOADING ON SPHERE

The problem considered in this report is illustrated in figure 1, which shows a spherical shell with a current-carrying wire attached to the surface along a great circle. The arrows on the wire indicate the direction of current flow and the arrow at b

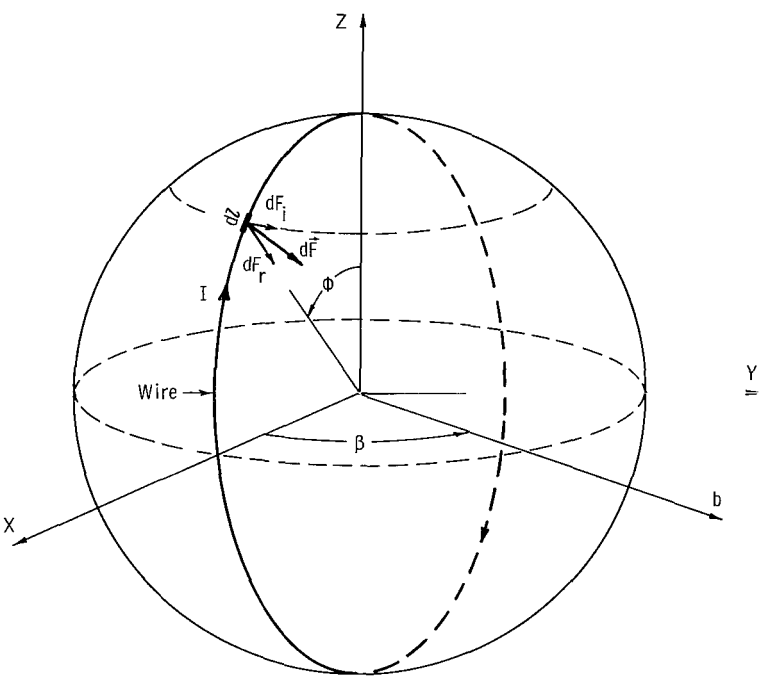

Figure 1.- Thin-walled spherical satellite with current-carrying wire attached to surface along a great circle.

indicates the direction of the geomagnetic field. The interaction of the current flowing in the wire with the geomagnetic field produces a force on the wire. The magnitude and direction of this force is given by the vector equation (see ref. 3)

$$d\vec{F} = \vec{I} \times \vec{B}\, dl \tag{1}$$

in which

$d\vec{F}$ differential force, newtons

$\vec{I}$ current in wire, amperes

$\vec{B}$ flux density of earth's magnetic field, webers per square meter

$d\ell$ differential length along wire, meters

The differential force $d\vec{F}$ can be divided into a component dF_i which lies in the plane of the sphere and a component dF_r which is directed normal to the surface of the sphere, or radially. The magnitude of the in-plane component dF_i is given by the scalar relation

$$dF_i = IB\, d\ell \cos \beta \sin \phi \tag{2}$$

whereas the out-of-plane, or radial, component dF_r is given by

$$dF_r = IB\, d\ell \sin \beta \tag{3}$$

An octant of the sphere of figure 1 is shown in greater detail in figure 2. Spherical coordinates ϕ and θ are used to locate a point on the surface of the sphere. The meridional angle ϕ is measured from the Z-axis, which passes through the upper pole. The circumferential angle θ is measured from the X-Z plane, which is also the plane of the wire. Angle β is the angle between the plane of the wire and the direction of the geomagnetic field, axis b. Axis b lies in the X-Y plane so that angle β is measured in the same way that angle θ is measured.

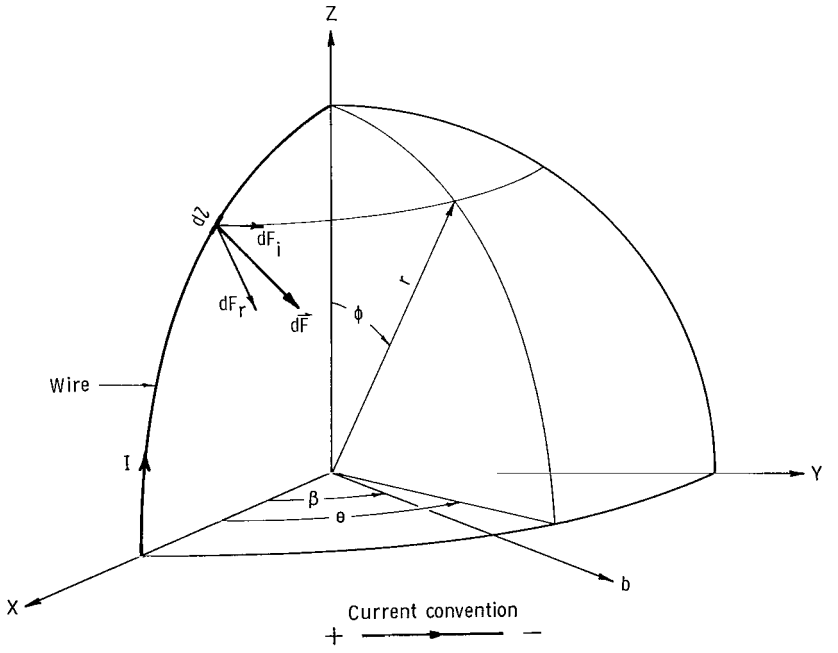

Figure 2.- Octant of sphere with current-carrying wire showing differential loading and spherical coordinates.

If both the angle β and the direction of the current I flowing in the wire are as shown in figures 1 and 2, then the radial force dF_r, which is independent of ϕ, is directed inward and the in-plane force dF_i is directed in the θ direction.

In this report only the in-plane component of the loading is considered. The constant radial component is treated on page 338 of reference 4. Since linear theory is used in reference 4 and in the present report, the effects of the two loadings may be superimposed.

The in-plane line load per unit length, $dF_i/d\ell$, introduced into the shell by the current-carrying wire may be written as

$$\frac{dF_i}{d\ell} = A \sin \phi \tag{4}$$

where, from equation (2),

$$A = IB \cos \beta \tag{5}$$

This applied sinusoidal line load (illustrated in fig. 3) gives a resultant torque T on the shell of magnitude

$$T = \int_0^{2\pi} Ar^2 \sin^2 \phi \, d\phi = Ar^2 \pi \tag{6}$$

From Newton's second law, for rotational motion,

$$T = I_\rho \alpha = \frac{8}{3} \pi r^4 \rho \alpha \tag{7}$$

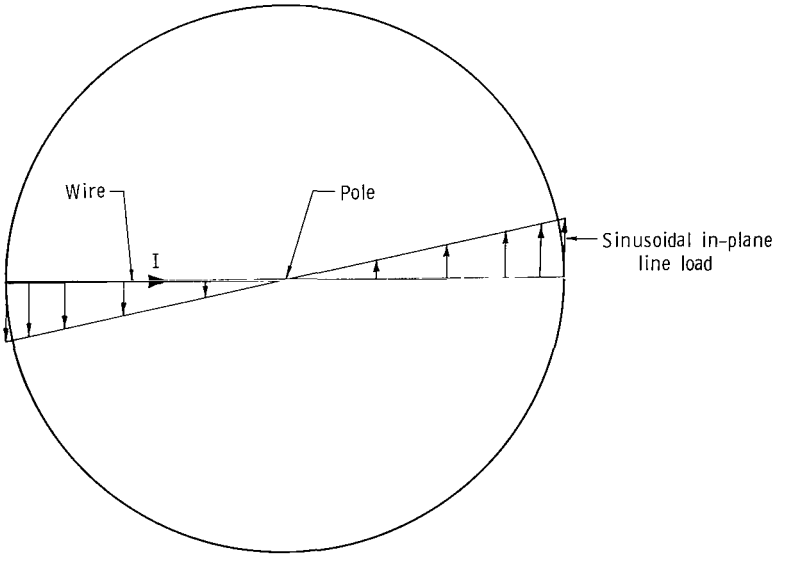

Figure 3.- Sinusoidal in-plane line load acting along a great circle of a sphere, causing a resultant applied torque. Top view.

Thus, the angular acceleration is

$$\alpha = \frac{3A}{8r^2\rho} \tag{8}$$

The applied torque is equilibrated by an inertia loading which is distributed over the surface of the shell and which is given by

$$P_\theta = -\rho r \alpha \sin \phi \tag{9}$$

or, using the value of α just calculated,

$$P_\theta = -\frac{3A}{8r} \sin \phi \tag{10}$$

Thus, the in-plane line load (eq. (4)) and the surface inertia load (eq. (9)) have been expressed as a function of the strength of the geomagnetic field, the amount of current flowing in the wire, the orientation of the wire with respect to the geomagnetic field, the radius of the spherical shell, the mass density of the sphere, and the position on the sphere.

SOLUTION OF MEMBRANE SHELL EQUATIONS

Equilibrium Equations and Stress Boundary Conditions

Because of the nature of the loading (all forces tangential to the surface) linear membrane shell theory is assumed to be adequate for investigating the stresses and deformations in the present problem. The coordinate system and a loaded shell element are shown in figures 2 and 4, respectively. The applied in-plane line load acts in the θ-direction along the great circle $\theta = 0$ and $\theta = \pi$.

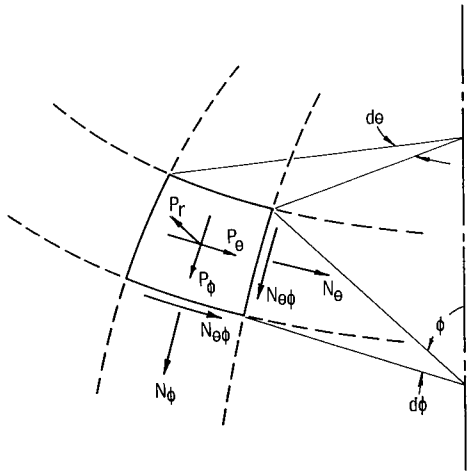

Figure 4.- Element of a loaded spherical shell.

From reference 5 the equilibrium equations for a nonaxisymmetrically loaded spherical membrane are given by

$$\frac{\partial N_\theta}{\partial \theta} + \frac{\partial N_{\theta\phi}}{\partial \phi} \sin \phi + 2N_{\theta\phi} \cos \phi + P_\theta r \sin \phi = 0 \tag{11}$$

$$\frac{\partial N_{\theta\phi}}{\partial \theta} - N_\theta \cos \phi + \frac{\partial N_\phi}{\partial \phi} \sin \phi + N_\phi \cos \phi + P_\phi r \sin \phi = 0 \tag{12}$$

$$N_\theta + N_\phi = rP_r \tag{13}$$

These equations represent three equations in the three unknown stress resultants N_θ, N_ϕ, and $N_{\theta\phi}$ which are to be solved in the region $0 \leqq \theta \leqq \pi$, $0 \leqq \phi \leqq \pi$. For the problem considered herein, $P_r = P_\phi = 0$; therefore, $N_\phi = -N_\theta$.

A complete set of boundary conditions can be written for $\theta = 0,\pi$ and $\phi = 0,\pi$. From symmetry conditions and from consideration of the applied loading given by equation (4), boundary conditions on N_θ can be written along $\theta = 0,\pi$. The remaining conditions, those on N_ϕ (which is equal to $-N_\theta$) and $N_{\theta\phi}$ along $\phi = 0,\pi$ and those on $N_{\theta\phi}$ along $\theta = 0,\pi$, are derived in appendix B. A summary of the stress boundary conditions is as follows:

Along $\theta = 0$,

$$N_\theta = -\frac{A}{2}\sin\phi \tag{14}$$

$$N_{\theta\phi} = \frac{3}{8}A\cos\phi \tag{15}$$

Along $\theta = \pi$,

$$N_\theta = \frac{A}{2}\sin\phi \tag{16}$$

$$N_{\theta\phi} = \frac{3}{8}A\cos\phi \tag{17}$$

Along $\phi = 0$,

$$N_\phi = -N_\theta = \frac{3}{8}A\sin 2\theta \tag{18}$$

$$N_{\theta\phi} = \frac{3}{8}A\cos 2\theta \tag{19}$$

Along $\phi = \pi$,

$$N_\phi = -N_\theta = \frac{3}{8}A\sin 2\theta \tag{20}$$

$$N_{\theta\phi} = -\frac{3}{8}A\cos 2\theta \tag{21}$$

In addition, symmetry conditions provide knowledge of certain stresses along $\theta = \frac{\pi}{2}$ and $\phi = \frac{\pi}{2}$ as follows:

Along $\theta = \frac{\pi}{2}$,

$$N_\theta = 0 \tag{22}$$

Along $\phi = \frac{\pi}{2}$,

$$N_{\theta\phi} = 0 \tag{23}$$

Stresses

Solution for the stress resultant N_θ.- The governing partial differential equation obtained by eliminating N_ϕ and $N_{\theta\phi}$ from the three equilibrium equations is

$$\frac{\partial^2 N_\theta}{\partial \theta^2} + 5 \sin \phi \cos \phi \frac{\partial N_\theta}{\partial \phi} + \left(4 \cos^2\phi - 2 \sin^2\phi\right) N_\theta + \sin^2\phi \frac{\partial^2 N_\theta}{\partial \phi^2} = 0 \qquad (24)$$

With first and second derivatives replaced by two- and three-point central-difference approximations, respectively, equation (24) may be written in difference form as

$$\frac{N_\theta(\theta+\Delta\theta,\phi) - 2N_\theta(\theta,\phi) + N_\theta(\theta-\Delta\theta,\phi)}{(\Delta\theta)^2} + \frac{N_\theta(\theta,\phi+\Delta\phi) - N_\theta(\theta,\phi-\Delta\phi)}{2\Delta\phi} 5 \sin \phi \cos \phi$$

$$+ N_\theta(\theta,\phi)\left[4 \cos^2\phi - 2 \sin^2\phi\right] + \frac{N_\theta(\theta,\phi+\Delta\phi) - 2N_\theta(\theta,\phi) + N_\theta(\theta,\phi-\Delta\phi)}{(\Delta\phi)^2} \sin^2\phi = 0 \qquad (25)$$

An iteration technique known as successive overrelaxation (ref. 6) is applied to equation (25) in the region $0 \leq \theta \leq \pi/2$, $0 \leq \phi \leq \pi$. The boundary conditions on N_θ are given in equations (14), (18), (20), and (22). Equation (25) written in successive over-relaxation form is

$$N_\theta^{(n+1)}(\theta,\phi) = \frac{-\omega}{-\frac{2}{(\Delta\theta)^2} + 4 \cos^2\phi - 2 \sin^2\phi - \frac{2 \sin^2\phi}{(\Delta\phi)^2}} \left\{ \left[N_\theta^{(n)}(\theta+\Delta\theta,\phi) + N_\theta^{(n+1)}(\theta-\Delta\theta,\phi) \right] \frac{1}{(\Delta\theta)^2} \right.$$

$$+ N_\theta^{(n)}(\theta,\phi+\Delta\phi)\left[\frac{5 \sin \phi \cos \phi}{2\Delta\phi} + \frac{\sin^2\phi}{(\Delta\phi)^2}\right]$$

$$\left. + N_\theta^{(n+1)}(\theta,\phi-\Delta\phi)\left[-\frac{5 \sin \phi \cos \phi}{2\Delta\phi} + \frac{\sin^2\phi}{(\Delta\phi)^2}\right] \right\} - (\omega - 1) N_\theta^{(n)}(\theta,\phi) \qquad (26)$$

in which ω is the relaxation factor and the superscript n refers to the value of N_θ obtained on the nth iteration. The purpose of the relaxation factor ω is to speed up convergence of the procedure. With $\omega = 1.0$ the method reduces to the better known but more slowly converging Gauss-Seidel iteration technique. The determination of an appropriate value for ω is discussed in reference 6. For the calculations performed in this study the value $\omega = 1.95$ was used. In the form given by equation (26), the computation is initiated at the point ($\theta=\Delta\theta$, $\phi=\Delta\phi$), which is one station to the right of the $\theta = 0$ boundary, and proceeds in the θ direction to the point $\left(\theta=\frac{\pi}{2}-\Delta\theta,\ \phi=\Delta\phi\right)$, which is one station to the left of the $\theta = \frac{\pi}{2}$ boundary. The coordinate ϕ is then increased by the increment $\Delta\phi$ and the computation again proceeds from $\theta = \Delta\theta$ to $\theta = \frac{\pi}{2} - \Delta\theta$.

This procedure is repeated until equation (26) has been applied to all points in the region $0 < \theta < \frac{\pi}{2}$, $0 < \phi < \pi$. In the present problem, a linear distribution in the θ direction using the values of N_θ along the lines $\theta = 0$ and $\theta = \frac{\pi}{2}$ was used as an initial approximation to start the computation. The complete cycle is repeated until convergence is obtained.

A contour plot of N_θ/A is shown in figure 5 and the values are given in table I.

For more details concerning methods of solution and for estimates of the accuracy of all stress and displacement results, see appendix C.

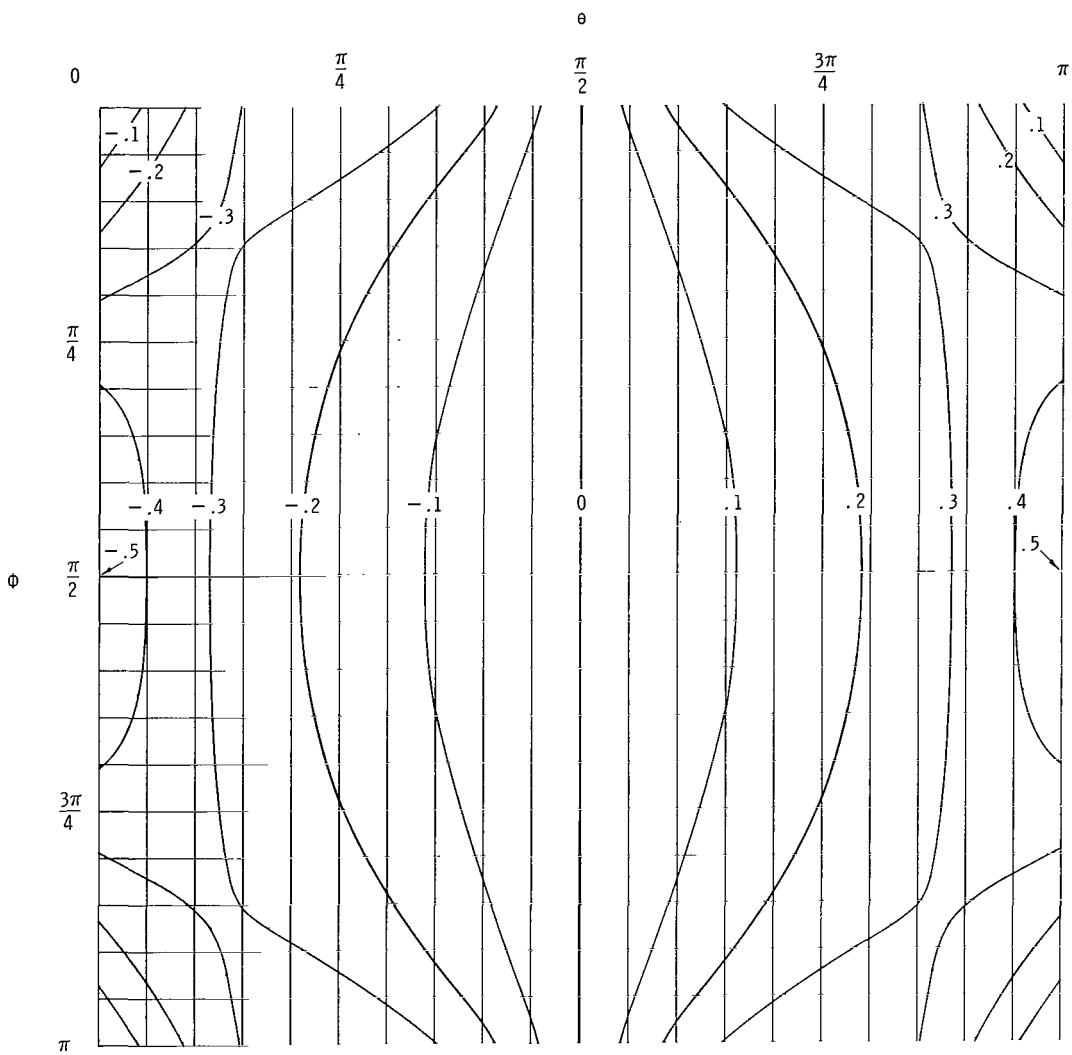

Figure 5.- Contour plot of $\frac{N_\theta}{A}$ in the hemispherical region $0 \leq \theta \leq \pi$, $0 \leq \Phi \leq \pi$.

Solution for the stress resultant $N_{\theta\phi}$.- Equation (11) can be used to determine $N_{\theta\phi}$. Introducing into equation (11) the expression for P_θ given in equation (10) and dividing the equation by $\sin \phi$ yields

$$\frac{\partial N_{\theta\phi}}{\partial \phi} = \frac{3A}{8} \sin \phi - \frac{1}{\sin \phi} \frac{\partial N_\theta}{\partial \theta} - 2N_{\theta\phi} \frac{\cos \phi}{\sin \phi} \tag{27}$$

Equation (27) is integrated numerically in the ϕ direction for $N_{\theta\phi}$ by using a Runge-Kutta method (ref. 7) for each value of θ. The derivative $\partial N_\theta / \partial \theta$ is evaluated numerically by using the N_θ distribution stored in the computer. A contour plot of $N_{\theta\phi}/A$ is shown in figure 6, and the values are given in table I.

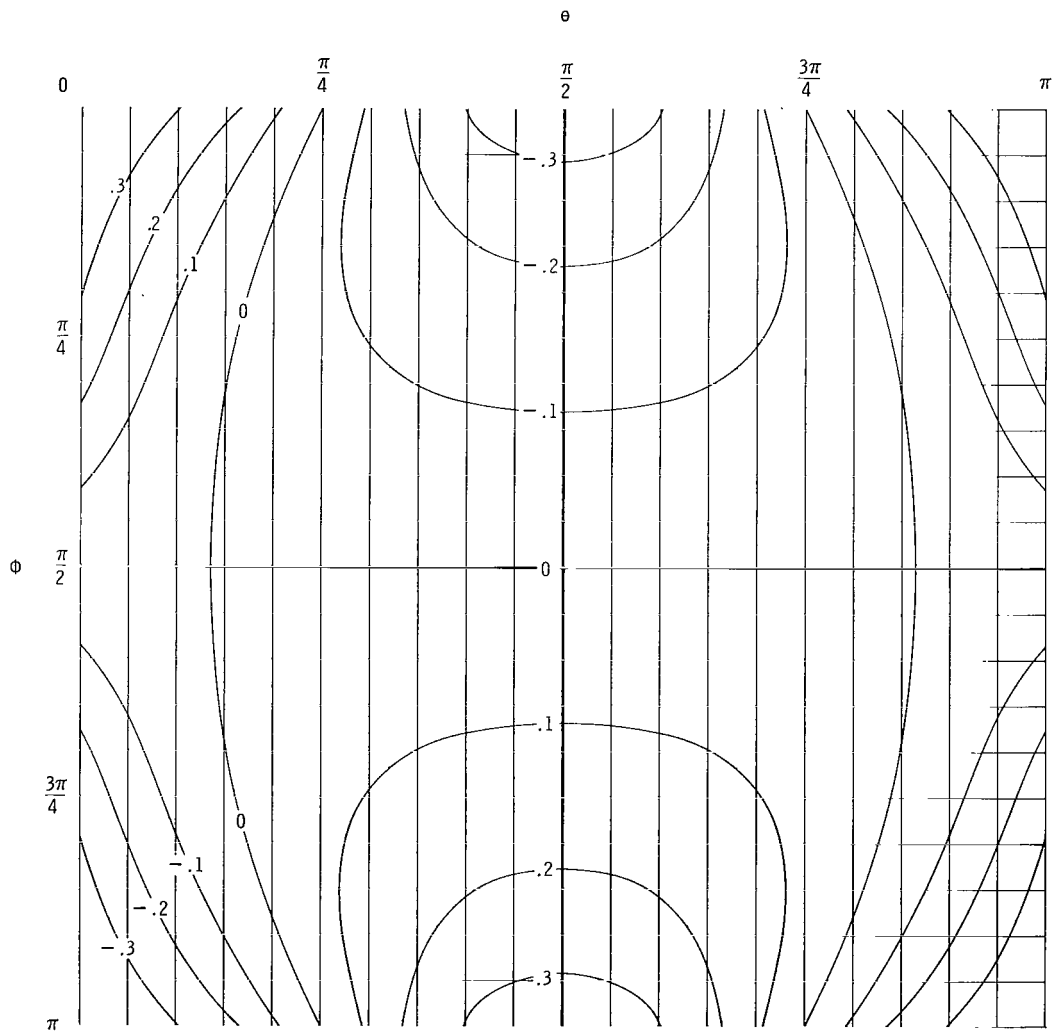

Figure 6.- Contour plot of $\frac{N_{\theta\Phi}}{A}$ in the hemispherical region $0 \leqq \theta \leqq \pi$, $0 \leqq \Phi \leqq \pi$.

Principal stress resultant N_n.- By making use of the fact that $N_\phi = -N_\theta$, the principal stress resultant N_n can be calculated from the equation

$$N_n = \left(N_\theta^2 + N_{\theta\phi}^2\right)^{1/2} \tag{28}$$

The values of the nondimensionalized principal stress resultant N_n/A are shown as a contour plot in figure 7 and are given in table I.

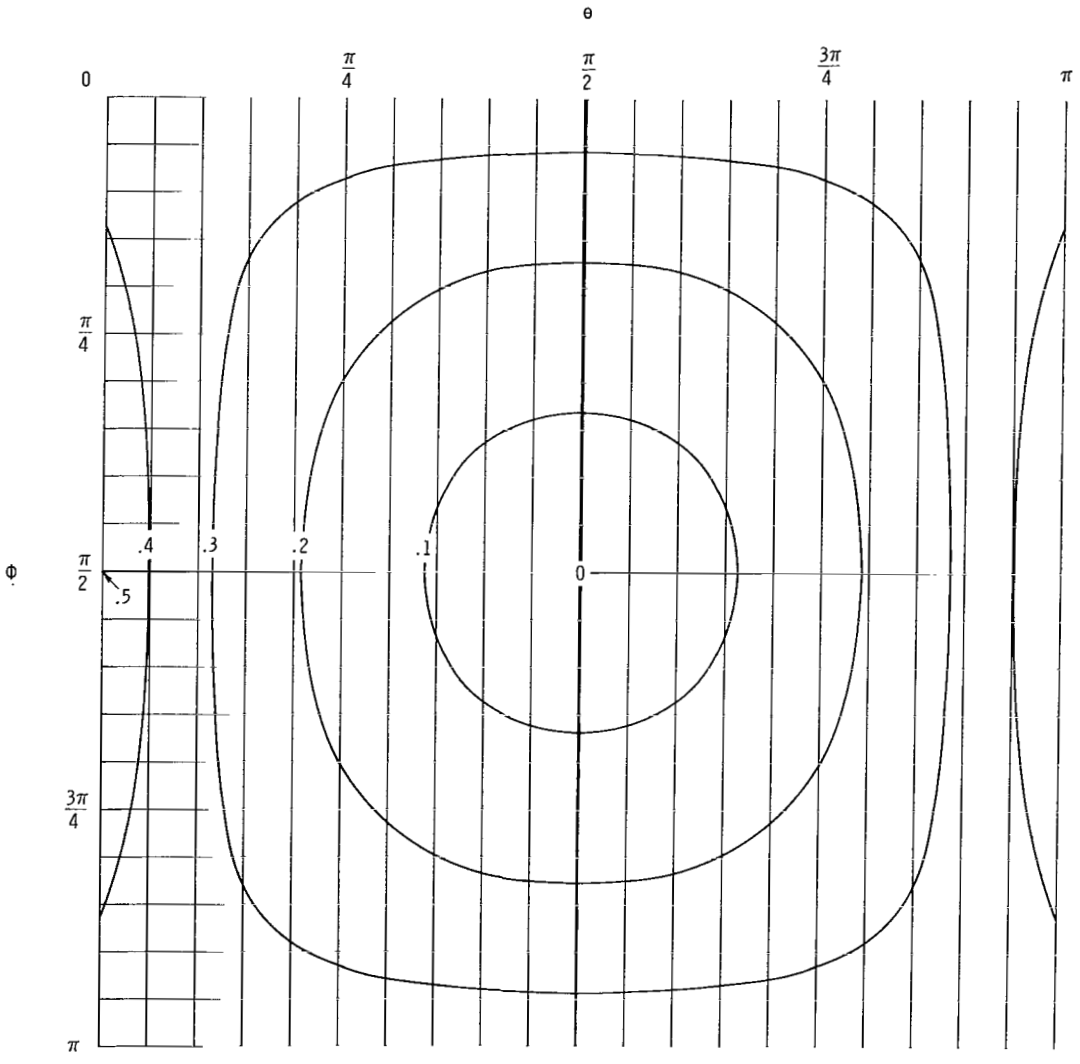

Figure 7.- Contour plot of $\frac{N_n}{A}$ in the hemispherical region $0 \leq \theta \leq \pi$, $0 \leq \Phi \leq \pi$.

Displacements

The displacements u, v, and w in the θ, ϕ, and radial directions, respectively, are shown in figure 8. They are calculated by using the following strain-displacement relations (ref. 4, p. 96):

$$\frac{\partial v}{\partial \phi} + w = r\epsilon_{\phi} \tag{29}$$

$$\frac{\partial u}{\partial \theta} + v \cos \phi + w \sin \phi = r\epsilon_{\theta} \sin \phi \tag{30}$$

$$\frac{\partial u}{\partial \phi} \sin \phi - u \cos \phi + \frac{\partial v}{\partial \theta} = r\gamma_{\theta\phi} \sin \phi \tag{31}$$

The strains may be expressed in terms of the stresses by using

$$\epsilon_{\phi} = \frac{1}{Et}\left(N_{\phi} - \mu N_{\theta}\right) = -\frac{1 + \mu}{Et} N_{\theta} \tag{32}$$

$$\epsilon_{\theta} = \frac{1}{Et}\left(N_{\theta} - \mu N_{\phi}\right) = \frac{1 + \mu}{Et} N_{\theta} \tag{33}$$

$$\gamma_{\theta\phi} = \frac{2(1 + \mu)}{Et} N_{\theta\phi} \tag{34}$$

The extreme right-hand sides of (32) and (33) were obtained by using $N_{\phi} = -N_{\theta}$.

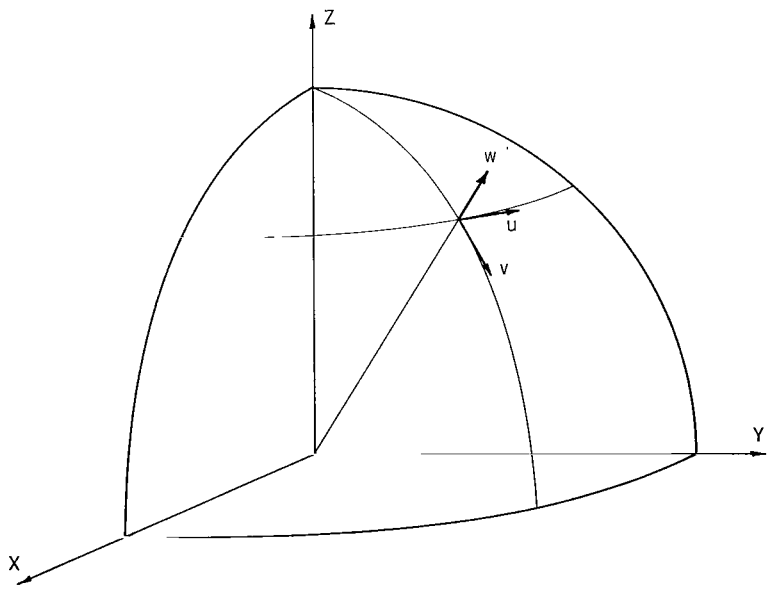

Figure 8.- Displacements u, v, and w in the θ, Φ, and radial directions, respectively, of a point on the surface of a sphere.

Solution for the displacements v and w.- The governing partial differential equation for v is obtained from equations (29) to (34) and is given by

$$\frac{\partial^2 v}{\partial \phi^2} \sin^2\phi - \frac{\partial v}{\partial \phi} \sin\phi \cos\phi + v + \frac{\partial^2 v}{\partial \theta^2} = -r \sin^2\phi \frac{2(1+\mu)}{Et} \frac{\partial N_\theta}{\partial \phi} + r \sin\phi \frac{2(1+\mu)}{Et} \frac{\partial N_{\theta\phi}}{\partial \theta} \tag{35}$$

By making use of equilibrium equations (11), (12), and (13) the right-hand side of (35) can be changed to give

$$\frac{\partial^2 v}{\partial \phi^2} \sin^2\phi - \frac{\partial v}{\partial \phi} \sin\phi \cos\phi + v + \frac{\partial^2 v}{\partial \theta^2} = \frac{4r(1+\mu)}{Et} N_\theta \sin\phi \cos\phi \tag{36}$$

The boundary conditions for v, which may be obtained from symmetry and antisymmetry conditions, are as follows:

Along $\theta = 0, \frac{\pi}{2}$,

$$v = 0 \tag{37}$$

Along $\phi = 0, \frac{\pi}{2}$,

$$v = 0 \tag{38}$$

The displacement v is calculated in the same way that the stress resultant N_θ is calculated – by the successive-overrelaxation method. The displacement w is calculated from equation (29). Contour plots of $vEt/rA(1+\mu)$ and $wEt/rA(1+\mu)$ are shown in figures 9 and 10, respectively, and the values are given in table I.

Solution for the displacement $u/\sin\phi$.- Rather than solving for the displacement u in the θ direction, it seems preferable to solve for $\bar{u} = \frac{u}{\sin\phi}$. The displacement u is less useful than $\bar{u}$ because u would be zero at $\phi = 0$ and $\phi = \pi$ even if a rigid-body rotation in the θ-direction were allowed. The quantity $\bar{u}/r$ is the angle of rotation in the θ-direction of a point on the shell as the shell deforms. At the pole $\phi = 0$, the quantity $\bar{u}/r$ is the angle of rotation of a line element passing through the pole. The equation for $\bar{u}$ is obtained from equation (31) and is given by

$$\frac{\partial \bar{u}}{\partial \phi} = \frac{-\frac{\partial v}{\partial \theta} + \frac{2r(1+\mu)}{Et} N_{\theta\phi} \sin\phi}{\sin^2\phi} \tag{39}$$

The behavior of $\partial\bar{u}/\partial\phi$ at the pole $\phi = 0$ is investigated by expressing the numerator and denominator on the right-hand side of equation (39) in powers of ϕ. The distribution of $\bar{u}$ at $\phi = 0$ is determined by expressing the terms in equation (30) in powers of ϕ. The resulting values of $\partial\bar{u}/\partial\phi$ and $\bar{u}$ at the pole are

$$\frac{\partial \bar{u}}{\partial \phi} = -\frac{rA(1+\mu)}{4Et}(\sin\theta + \sin 3\theta) \qquad (\phi = 0) \qquad (40)$$

$$\bar{u} = \frac{3rA(1+\mu)}{8Et}\cos 2\theta \qquad (\phi = 0) \qquad (41)$$

Because of the difficulty of accurately evaluating the right-hand side of equation (39) near (but not at) the pole, interpolation formulas are used in that region. See appendix C for details.

With the above information it is possible to solve for $\bar{u}$ by using equation (39) and a Runge-Kutta method. A contour plot of $uEt/rA(1+\mu)\sin\phi$ is shown in figure 11 and the values are given in table I.

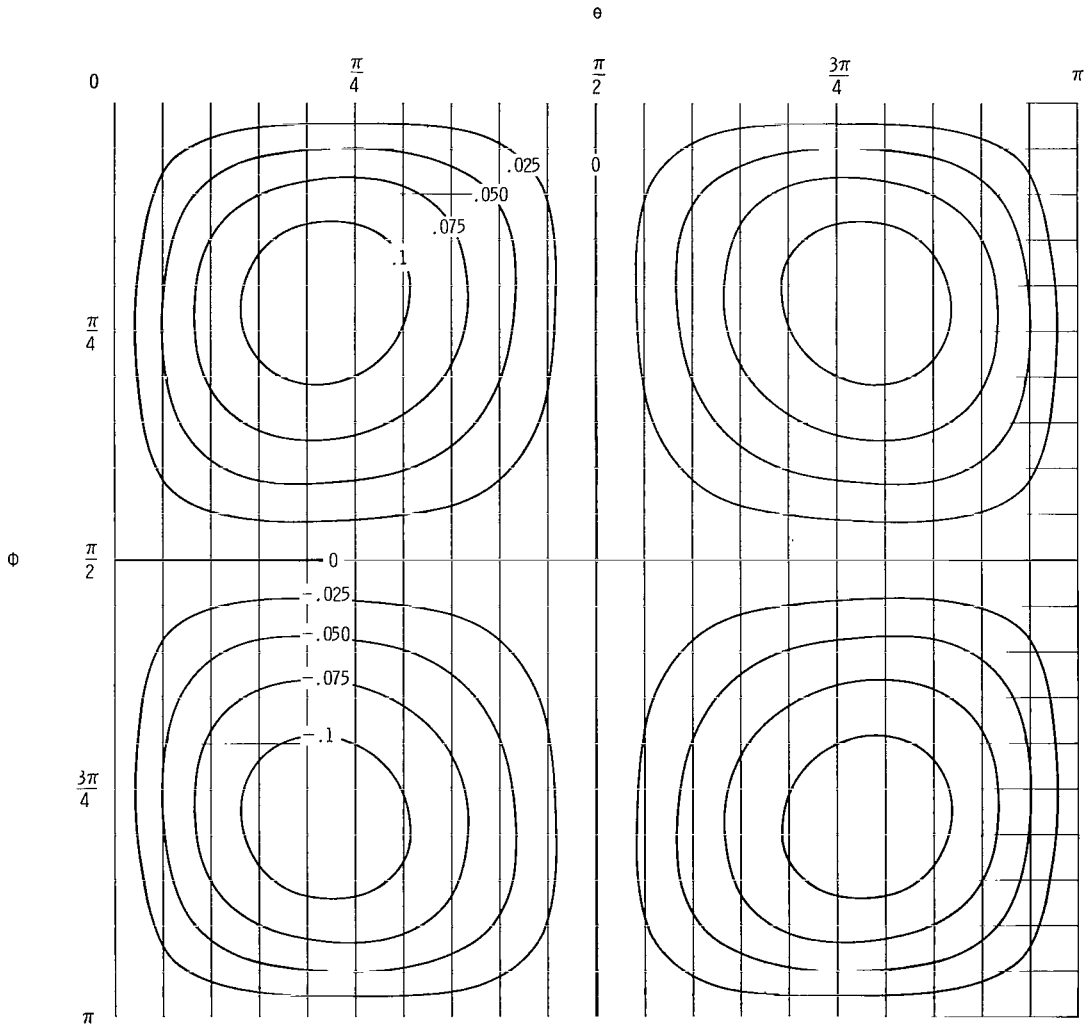

Figure 9.- Contour plot of $\frac{vEt}{rA(1+\mu)}$ in the hemispherical region $0 \leq \theta \leq \pi$, $0 \leq \Phi \leq \pi$.

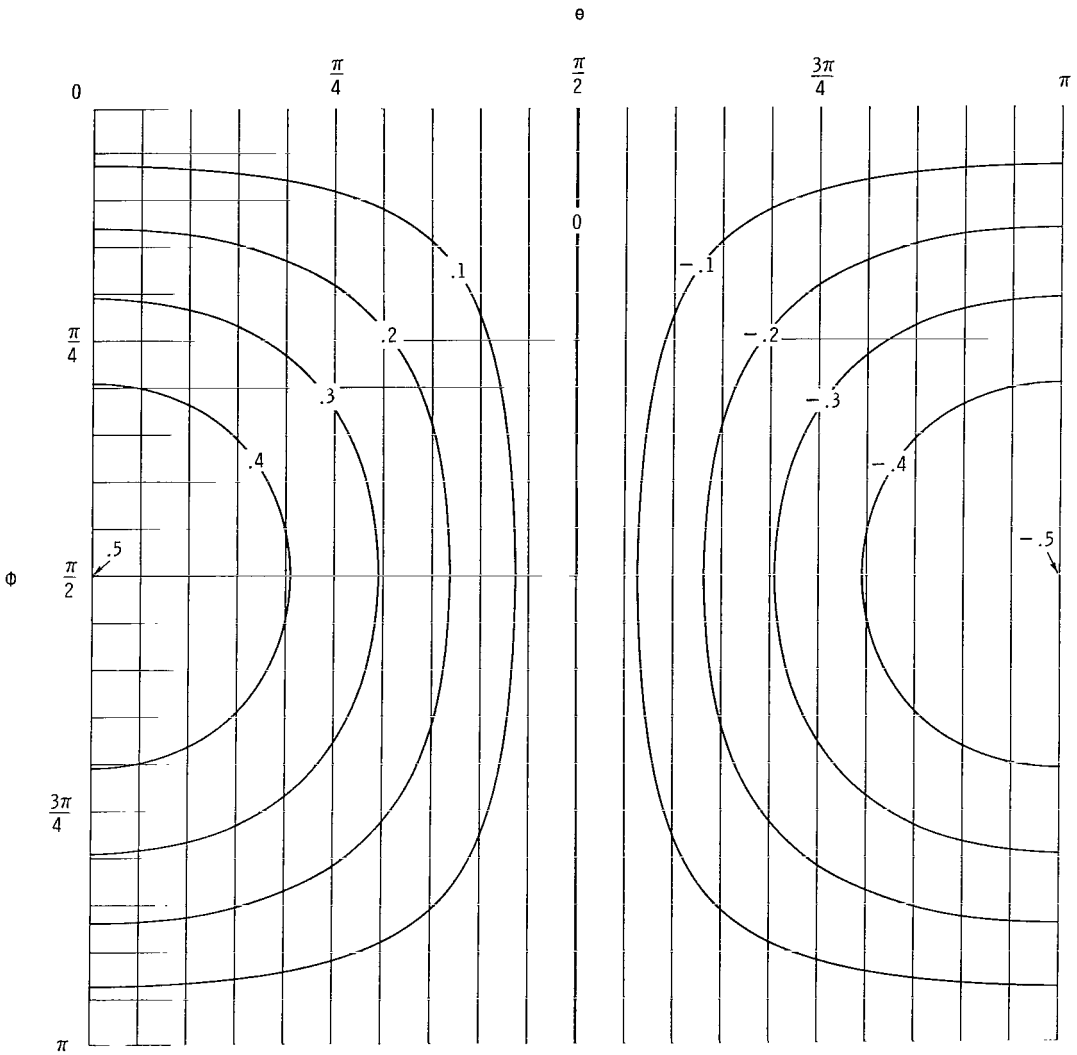

Figure 10.- Contour plot of $\frac{wEt}{rA(1+\mu)}$ in the hemispherical region $0 \leq \theta \leq \pi$, $0 \leq \Phi \leq \pi$.

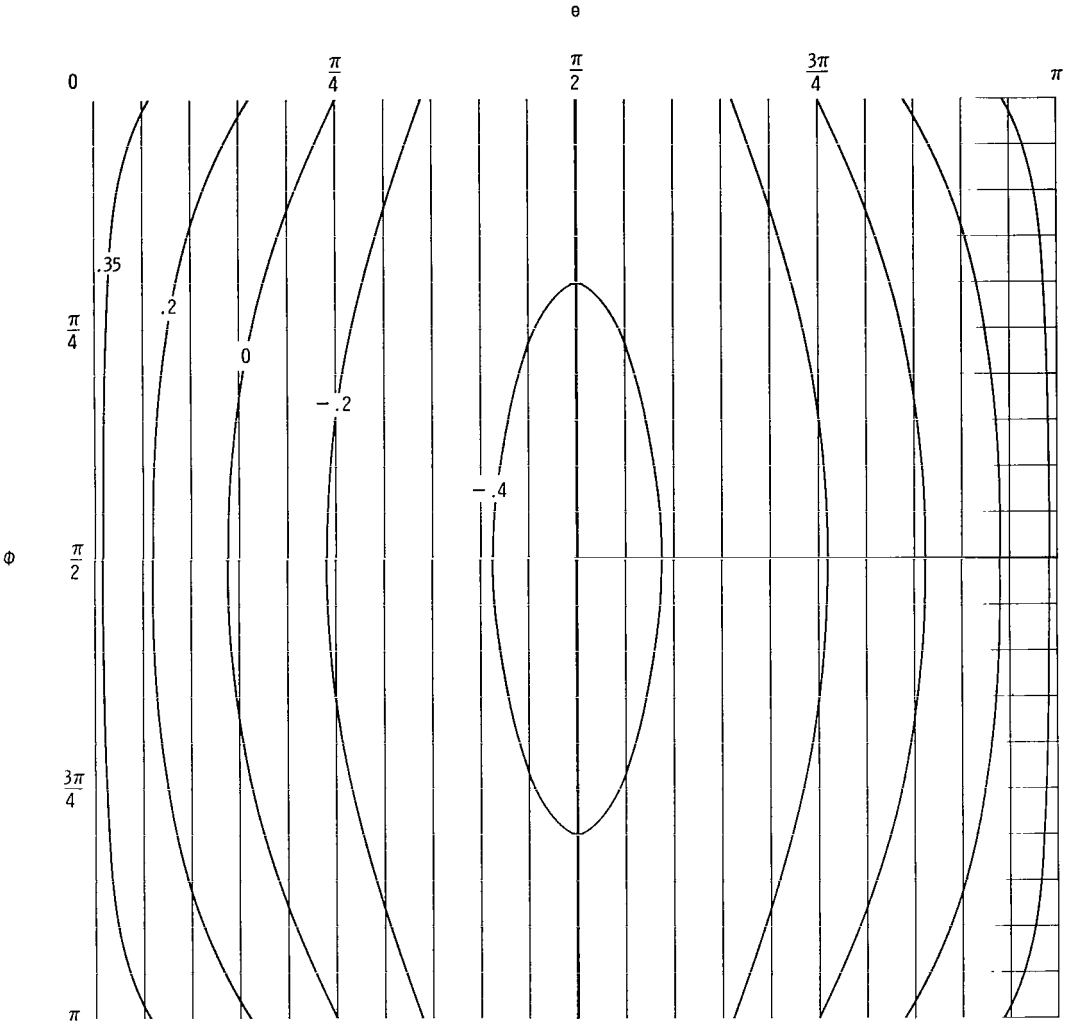

Figure 11.- Contour plot of $\frac{uEt}{rA(1 + \mu)\sin \Phi}$ in the hemispherical region $0 \leq \theta \leq \pi$, $0 \leq \Phi \leq \pi$.

DISCUSSION OF RESULTS

Contour plots of $\frac{N_\theta}{A}$, $\frac{N_{\theta\phi}}{A}$, $\frac{N_n}{A}$, $\frac{vEt}{rA(1+\mu)}$, $\frac{wEt}{rA(1+\mu)}$, and $\frac{uEt}{rA(1+\mu)\sin\phi}$ are shown in figures 5, 6, 7, 9, 10, and 11, respectively, and the values of these nondimensionalized stress resultants and displacements are given in table I. The inadequacy of linear membrane theory near the line loads is apparent in that the displacement w is discontinuous at the line loads $\theta = 0$ and $\theta = \pi$. In the regions near the lines $\theta = 0$ and $\theta = \pi$, bending occurs and/or nonlinear membrane action is present which, because of antisymmetry, would cause w to be zero. These linear membrane theory results are expected to be correct a short distance away from the line loads.

Inasmuch as the station-keeping method referred to herein would be applied to very thin Echo-like satellites which carry no internal pressure, the compressive stresses caused by the line loads might bring about buckling of the surface. The magnitude of the load that would cause buckling can be approximated by making use of results of buckling tests on similar spheres presented in reference 8. The uniform pressure differential that caused buckling in a 12.5-ft (3.81-m) diameter sphere of aluminum foil-Mylar laminate was about 14 percent of the classical buckling pressure differential of

$$\Delta p_{cl} = \left(\frac{2}{r}\right)^2 \sqrt{DK} \tag{42}$$

where D is the bending stiffness and K is the extensional stiffness of the laminate.

The stress resultant N_n caused by this pressure differential is

$$N_{n,cl} = \frac{\Delta p_{cl} r}{2} \tag{43}$$

For the problem of a line load on a sphere considered in this report, the maximum value of the principal stress N_n is $A/2$ and occurs at the points $\left(\theta = 0,\ \phi = \frac{\pi}{2}\right)$ and $\left(\theta = \pi,\ \phi = \frac{\pi}{2}\right)$. If it is assumed that the surface of the sphere buckles at the same maximum stress level under a nonuniform in-plane load as under uniform external pressure, then local buckling is initiated when

$$N_{n,max} = \frac{A}{2} = \frac{0.14\left(\frac{2}{r}\right)^2 \sqrt{DK}\, r}{2} \tag{44}$$

From equation (8), the angular acceleration α is related to the constant A by

$$\alpha = \frac{3A}{8r^2\rho} \tag{45}$$

The values of A and α which cause buckling are now calculated for the cases of a 12.5-ft (3.81-m) diameter sphere and a 135-ft (41.2-m) diameter sphere. For

each case the time t that is required to rotate the initially nonrotating sphere through an angle of $\pi/2$ radians is also calculated from the formula

$$\frac{\pi}{2} = \frac{1}{2}\alpha t^2 \tag{46}$$

Note that the value of the angular acceleration α given by equation (45) causes buckling of the surface of the sphere; therefore, it is considered the upper limit for α. If this constant limiting value of α is used in equation (46), the value of the time t is the minimum time required to rotate the sphere through an angle of $\pi/2$ radians.

Both spheres are assumed to be fabricated of the aluminum foil-Mylar laminate discussed in reference 8. For this material, which is nominally identical to that used in Echo A-12 (Echo II), the material properties are

$$D = 23.8 \times 10^{-5} \text{ lbf-in.} \quad (2.69 \times 10^{-5} \text{ N-m})$$

$$K = 3055 \text{ lbf/in.} \quad (53.50 \times 10^{4} \text{ N/m})$$

$$\rho = 1.80 \times 10^{-6} \text{ slugs/in}^2 \quad (40.7 \text{ g/m}^2)$$

The values for D and K are taken from reference 8. Results for the two spheres are:

Case 1	Case 2
Diameter = 12.5 ft (3.81 m)	Diameter = 135 ft (41.2 m)
r = 75 in. (1.90 m)	r = 810 in. (20.6 m)
A = 0.00637 lbf/in. (1.11 N/m)	A = 0.00059 lbf/in. (0.103 N/m)
α = 2.83 rad/sec^2	α = 0.00225 rad/sec^2
t = 1.05 sec	t = 37.4 sec

These results indicate angular-acceleration limitations caused by geometrical and material factors. For the second case, corresponding to the Echo A-12 (Echo II) satellite, the minimum time required for rotation would not appear to impose any undue operational restrictions. However, other limitations may be associated with concentrated masses such as battery packs, tracking beacons, and other instrumentation attached to the surface of the sphere.

CONCLUDING REMARKS

Stress resultants and displacements have been calculated for a sinusoidal in-plane line load acting along a great circle of a spherical passive communications satellite. Linear membrane theory is used and, within the framework of this theory, other loadings may be superimposed on the given one. An example is presented of a thin-walled spherical satellite with a load applied which initiates local buckling at points on the surface of

the satellite. The results from this example indicate how the buckling strength of the structure may impose limitations on the maximum angular accelerations which can be applied to the satellite. Also, the results indicate that the order of magnitude of these limitations for a passive communications satellite of practical proportions is not prohibitive.

Langley Research Center,
National Aeronautics and Space Administration,
Langley Station, Hampton, Va., August 7, 1967,
124-08-06-02-23.

APPENDIX A

CONVERSION OF U.S. CUSTOMARY UNITS TO SI UNITS

The International System of Units (SI) was adopted by the Eleventh General Conference on Weights and Measures, Paris, October 1960, in Resolution No. 12 (ref. 2). Conversion factors for the units used herein are given in the following table:

Physical quantity	U.S. Customary Unit	Conversion factor (*)	SI Unit
Force	lbf	4.448222	newtons (N)
Length	in.	0.0254	meters (m)
Mass	slugs	14 593.90	grams (g)

*Multiply value given in U.S. Customary Unit by conversion factor to obtain equivalent value in SI unit.

APPENDIX B

THE DEVELOPMENT OF BOUNDARY CONDITIONS

Equation (24) is a partial differential equation of the second order in both θ and ϕ. The unknown in that equation is N_θ. It is also possible to manipulate equations (11), (12), and (13) to arrive at a similar equation with $N_{\theta\phi}$ as the unknown. In order to solve either of these two equations it is necessary to have four boundary conditions – two along θ boundaries and two along ϕ boundaries. At present, consider equation (24) with N_θ as the unknown (repeated here for convenience):

$$\frac{\partial^2 N_\theta}{\partial \theta^2} + 5 \sin \phi \cos \phi \frac{\partial N_\theta}{\partial \phi} + \left(4 \cos^2\phi - 2 \sin^2\phi\right) N_\theta + \sin^2\phi \frac{\partial^2 N_\theta}{\partial \phi^2} = 0 \qquad \text{(B1)}$$

The two boundary conditions which are given in equations (14) and (22) can be developed on the basis of symmetry conditions. These same two boundary conditions satisfy the requirement for two boundary conditions along θ boundaries and are given by

$$N_\theta = -\frac{A}{2} \sin \phi \qquad (\theta = 0) \qquad \text{(B2)}$$

$$N_\theta = 0 \qquad \left(\theta = \frac{\pi}{2}\right) \qquad \text{(B3)}$$

Symmetry of N_θ about the line $\phi = \frac{\pi}{2}$ can be used to satisfy one of the two boundary conditions along ϕ boundaries. The boundary condition which is needed is the distribution of N_θ at a pole $\phi = 0$ or $\phi = \pi$.

Let N_θ be expanded in a power series in ϕ as

$$N_\theta = N_{\theta,0} + N_{\theta,1}\phi + N_{\theta,2}\phi^2 + \ldots + N_{\theta,i}\phi^i + \ldots \qquad \text{(B4)}$$

in which the coefficients $N_{\theta,i}$ are functions of θ. These coefficients can be obtained by substituting equation (B4) into equation (B1) in which the trigonometric functions have also been expanded in powers of ϕ. After coefficients of like powers of ϕ are grouped, equation (B1) becomes

$$N''_{\theta,0} + 4N_{\theta,0} + \left(N''_{\theta,1} + 9N_{\theta,1}\right)\phi + \left(N''_{\theta,2} + 16N_{\theta,2} - 6N_{\theta,0}\right)\phi^2 + \ldots = 0 \qquad \text{(B5)}$$

It is valid to set equal to zero the coefficients of each power of ϕ in equation (B5). When this is done a set of ordinary differential equations is obtained, the first of which is

$$N''_{\theta,0} + 4N_{\theta,0} = 0 \qquad \text{(B6)}$$

APPENDIX B

The solution to equation (B6) is

$$N_{\theta,0} = a_1 \sin 2\theta + a_2 \cos 2\theta \tag{B7}$$

The boundary condition given by equation (B2) is also expanded in a power series. That series together with equation (B3) provides the following boundary conditions for $N_{\theta,0}$:

$$N_{\theta,0} = 0 \qquad (\theta = 0) \tag{B8}$$

$$N_{\theta,0} = 0 \qquad \left(\theta = \frac{\pi}{2}\right) \tag{B9}$$

The constant a_2 is therefore zero, but a_1 is undetermined. The distribution of N_θ at $\phi = 0$ is thus known, but the amplitude of that distribution is not known.

The two boundary conditions along ϕ boundaries which are required in order to obtain a solution to equation (B1) are thus

$$N_\theta = a_1 \sin 2\theta \qquad (\phi = 0, \pi) \tag{B10}$$

Suppose one arbitrarily assumes that a_1 is zero, uses that as the boundary condition at the upper and lower pole, and solves for the stress distribution N_θ using successive overrelaxation in the region $0 \leqq \theta \leqq \frac{\pi}{2}$, $0 \leqq \phi \leqq \pi$. Three examples of the results, which depend upon the grid size in the ϕ direction, are shown in figure 12. In each of the three cases the results exhibit wide oscillations very near the pole $\phi = 0$, but four

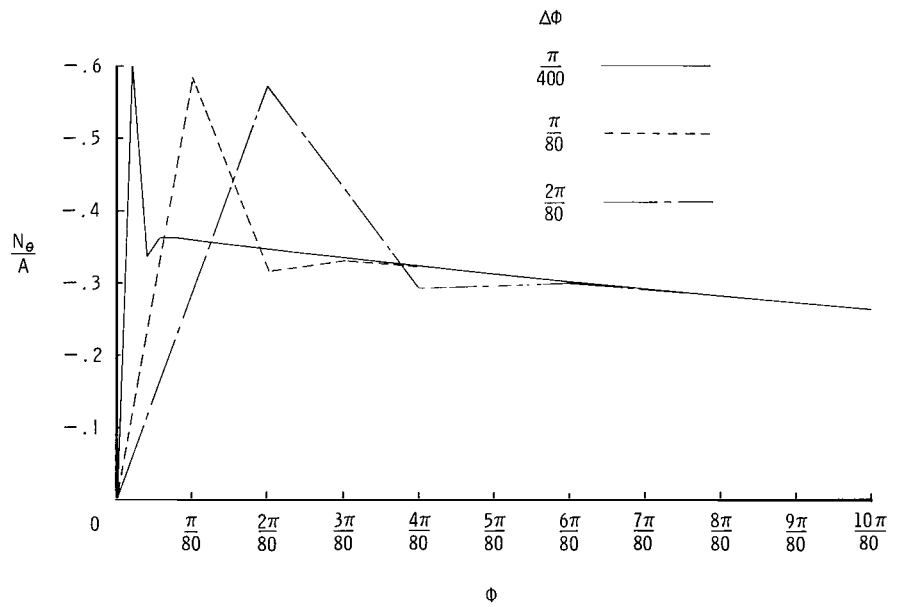

Figure 12.- The nondimensionalized stress $\frac{N_\theta}{A}$ near $\Phi = 0$ along the line $\theta = \frac{\pi}{4}$ for three values of $\Delta\Phi$. For all three cases $\frac{a_1}{A} = 0$.

or five stations away from the pole the solution converges to the correct value of N_θ regardless of the choice of $\Delta\phi$. This phenomenon is demonstrated again in figure 13, which shows the stress near the pole for three choices of a_1. These results suggest that the smoothness of the N_θ distribution near $\phi = 0$ can be used as a criterion for determining the correct value for a_1.

The value of a_1 can be determined to three places by using graphs similar to those shown in figures 12 and 13. More accuracy can be obtained by using several values of a_1 and calculating a table of N_θ differences for each value of a_1 used. The differences on N_θ can be taken in the ϕ-direction along the line $\theta = \frac{\pi}{4}$ in the neighborhood of the upper pole. By using smoothness in the differences as the criterion, the constant a_1/A was determined to be -0.37503 ± 0.00004. The uncertainty (±0.00004) arises because the digit in the last place is affected by the mesh size used to converge on the constant. That this value of a_1 is essentially correct can be ascertained by another method.

A top view of the loaded sphere divided along the line of action of the applied line load is shown in figure 14. Half the line load is assumed to be acting on the left hemisphere, and half on the right. The in-plane inertia load is represented by the arrows

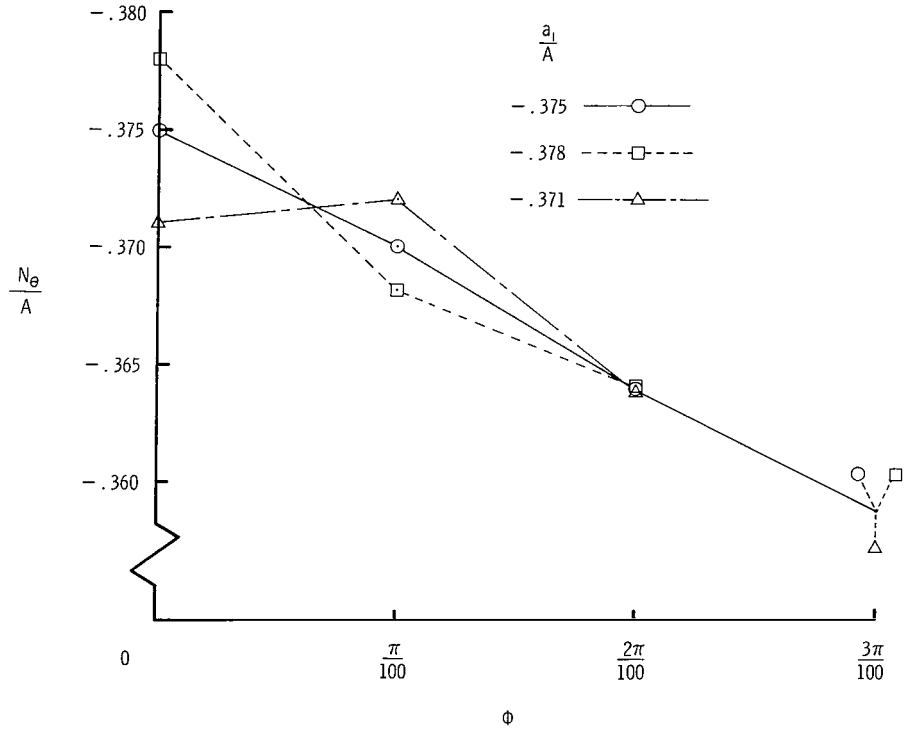

Figure 13.- The nondimensionalized stress $\frac{N_\theta}{A}$ near $\Phi = 0$ along the line $\theta = \frac{\pi}{4}$ for three values of $\frac{a_1}{A}$.

APPENDIX B

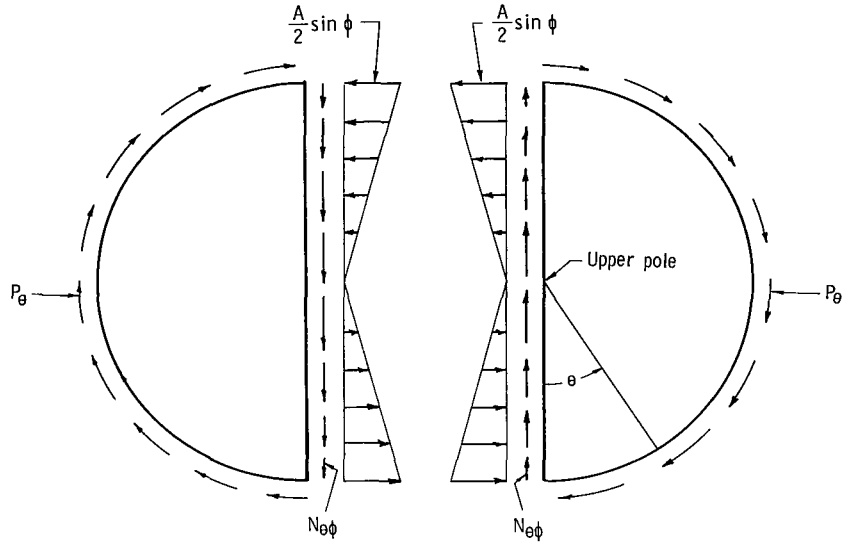

Figure 14.- Top view of loaded sphere divided along the line of action of the applied line load.

around the circumference. By considering the vertical* equilibrium of the hemisphere on the right, for example, it is possible to calculate the distribution of the shear stress along the cut which passes through the upper and lower poles. This knowledge provides the required boundary condition.

The vertical* resultant of the inertia load can be considered to be a shear load V given by

$$V = \int_0^{\pi} \int_0^{\pi} P_\theta r^2 \sin\phi \sin\theta \, d\theta \, d\phi \tag{B11}$$

$$= \frac{3}{8} Ar\pi \tag{B12}$$

The shear-stress distribution along the cut can be related to this shear load by using the familiar equation for the transverse shear-stress distribution in engineering beam theory:

$$b\tau = 2N_{\theta\phi} = \frac{VQ}{\hat{I}} \tag{B13}$$

where $b = 2t$, τ is the shear stress, and the cross section of the sphere is regarded as the cross section of an elementary beam.

*Vertical here means the vertical direction in figure 14, which is the x-direction.

APPENDIX B

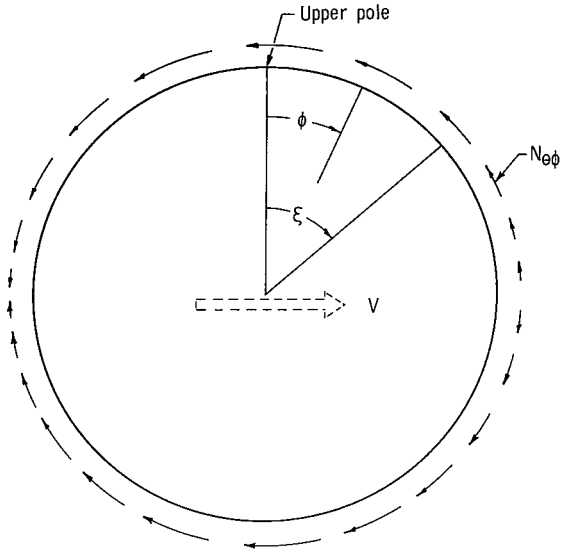

Figure 15.- Hemisphere showing resultant shear force V caused by in-plane inertia load P_θ and the equilibrating shear stress $N_{\theta\phi}$.

The right-hand hemisphere of figure 14 is shown in a view from center out in figure 15. The large arrow indicates the direction of the resultant shear force V. By using this figure it is seen that if the shear stress $N_{\theta\phi}$ is to be calculated at some point ϕ, then Q is the first moment of the material to the right of ϕ, the first moment being calculated with respect to the line $\phi = 0$. Thus

$$Q = 2\int_{\phi}^{\pi/2} tr^2 \sin \xi \, d\xi \qquad \text{(B14)}$$

$$= 2tr^2 \cos \phi \qquad \text{(B15)}$$

The quantity $\hat{I}$, the area moment of inertia of the cross section of the sphere about the line $\phi = 0$, is given by

$$\hat{I} = \pi r^3 t \qquad \text{(B16)}$$

By substituting equations (B12), (B15), and (B16) into (B13), the shear stress distribution along the line $\theta = 0$ is found to be

$$N_{\theta\phi} = \frac{3A}{8} \cos \phi \qquad \text{(B17)}$$

A shell element at the pole of the sphere, together with the positive directions for the stress resultants, is shown in figure 16. The values of the stress resultants along the line $\theta = 0$ are known: $N_{\theta\phi} = \frac{3A}{8} \cos \phi$, $N_\theta = -\frac{A}{2} \sin \phi$, and, in addition, $N_\phi = -N_\theta$ everywhere (from eq. (13)). Therefore, the stress resultants for an element in the orientation shown in figure 16 are known. By using the transformation equations for plane stress it is possible to obtain the stress at this same point for other orientations – that is, for other values of θ. The stress resultants as a function of θ at the point $\phi = 0$ are given by

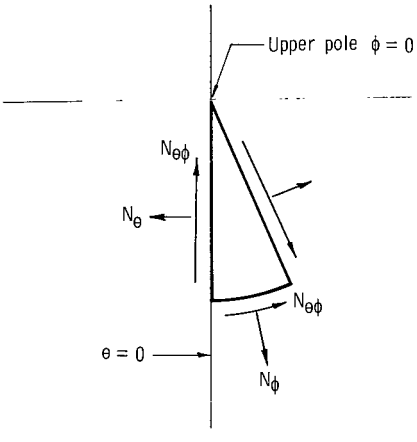

Figure 16.- Element at pole of sphere.

$$N_\theta = -\frac{3}{8} A \sin 2\theta \qquad \text{(B18)}$$

$$N_\phi = \frac{3}{8} A \sin 2\theta \qquad \text{(B19)}$$

$$N_{\theta\phi} = \frac{3}{8} A \cos 2\theta \qquad \text{(B20)}$$

APPENDIX B

A summary of the stress boundary conditions is

$$N_\theta = -\frac{3}{8} A \sin 2\theta \qquad (\phi = 0) \qquad \text{(B21)}$$

$$N_{\theta\phi} = \frac{3}{8} A \cos 2\theta \qquad (\phi = 0) \qquad \text{(B22)}$$

$$N_{\theta\phi} = 0 \qquad \left(\phi = \frac{\pi}{2}\right) \qquad \text{(B23)}$$

$$N_\theta = -\frac{A}{2} \sin \phi \qquad (\theta = 0) \qquad \text{(B24)}$$

$$N_\theta = 0 \qquad \left(\theta = \frac{\pi}{2}\right) \qquad \text{(B25)}$$

$$N_{\theta\phi} = \frac{3}{8} A \cos \phi \qquad (\theta = 0, \pi) \qquad \text{(B26)}$$

APPENDIX C

ACCURACY OF SOLUTION

Stress Resultant N_θ

The distribution for N_θ was calculated by using a five-point central-difference equation modified to make use of a successive overrelaxation technique. That difference equation (26) is repeated here:

$$N_\theta^{(n+1)}(\theta,\phi) = \frac{-\omega}{-\frac{2}{(\Delta\theta)^2} + 4\cos^2\phi - 2\sin^2\phi - \frac{2\sin^2\phi}{(\Delta\phi)^2}} \left\{ \left[N_\theta^{(n)}(\theta+\Delta\theta,\phi) + N_\theta^{(n+1)}(\theta-\Delta\theta,\phi) \right] \frac{1}{(\Delta\theta)^2} \right.$$

$$+ N_\theta^{(n)}(\theta,\phi+\Delta\phi) \left[\frac{5\sin\phi\cos\phi}{2\Delta\phi} + \frac{\sin^2\phi}{(\Delta\phi)^2} \right]$$

$$\left. + N_\theta^{(n+1)}(\theta,\phi-\Delta\phi) \left[-\frac{5\sin\phi\cos\phi}{2\Delta\phi} + \frac{\sin^2\phi}{(\Delta\phi)^2} \right] \right\} - (\omega - 1)N_\theta^{(n)}(\theta,\phi) \qquad \text{(C1)}$$

The boundary conditions are

$$N_\theta = -\frac{A}{2}\sin\phi \qquad (\theta = 0) \qquad \text{(C2)}$$

$$N_\theta = 0 \qquad \left(\theta = \frac{\pi}{2}\right) \qquad \text{(C3)}$$

$$N_\theta = -\frac{3A}{8}\sin 2\theta \qquad (\phi = 0,\ \pi) \qquad \text{(C4)}$$

The overrelaxation factor ω was approximated as 1.95. The mesh size used in the final computation was $\Delta\theta = \frac{\pi}{200}$ and $\Delta\phi = \frac{\pi}{160}$.

The degree of accuracy that could be expected from the numerically obtained N_θ distribution was ascertained by varying the mesh size in both the θ and ϕ directions and noting the digits which changed with the mesh size. Except near the pole $\left(0 < \phi < \frac{\pi}{20}\right)$ the changes in N_θ occurred in the sixth place. The results for N_θ presented in table I are believed to be correct to the number of digits retained.

Shear-Stress Resultant $N_{\theta\phi}$

The distribution of the shear-stress resultant $N_{\theta\phi}$ was calculated from the equilibrium equation (11), rewritten here in a slightly different form:

APPENDIX C

$$\frac{\partial N_{\theta\phi}}{\partial \phi} = \frac{3A}{8} \sin \phi - \frac{1}{\sin \phi} \frac{\partial N_{\theta}}{\partial \theta} - 2N_{\theta\phi} \frac{\cos \phi}{\sin \phi} \tag{C5}$$

The following boundary conditions are known:

$$N_{\theta\phi} = \frac{3A}{8} \cos 2\theta \qquad (\phi = 0) \tag{C6}$$

$$N_{\theta\phi} = 0 \qquad \left(\phi = \frac{\pi}{2}\right) \tag{C7}$$

The boundary condition (C7) was used to initiate the computation. Equation (C5) was integrated in the ϕ direction by using the following Runge-Kutta method (ref. 7):

$$y_{n+1} = y_n + \frac{k_1 + 2k_2 + 2k_3 + k_4}{6} + O\left(h^5\right) \tag{C8}$$

where

$$k_1 = hf\left(x_n, y_n\right)$$

$$k_2 = hf\left(x_n + \frac{h}{2}, y_n + \frac{k_1}{2}\right)$$

$$k_3 = hf\left(x_n + \frac{h}{2}, y_n + \frac{k_2}{2}\right)$$

$$k_4 = hf\left(x_n + h, y_n + k_3\right)$$

In the notation of the present problem,

$$y = N_{\theta\phi}$$

$$f = \frac{\partial N_{\theta\phi}}{\partial \phi}$$

$$x = \phi$$

$$h = 2\Delta\phi$$

where $\Delta\phi$ is the mesh size used in the N_θ calculation. The integration progressed from $\phi = \frac{\pi}{2}$ toward the pole.

Because it appeared that the error in this integration method was beginning to build up as the integration neared the upper pole, the values of $N_{\theta\phi}$ in the region $0 < \theta \leq \frac{\pi}{2}$, $\frac{\pi}{20} \leq \phi \leq \frac{2\pi}{20}$ were calculated by using equation (12), which, for the present problem, reduces to

$$\frac{\partial N_{\theta\phi}}{\partial \theta} = 2N_{\theta} \cos \phi + \frac{\partial N_{\theta}}{\partial \phi} \sin \phi \tag{C9}$$

APPENDIX C

The same Runge-Kutta method which was used to integrate equation (C5) in the ϕ-direction was also used to integrate equation (C9) in the θ-direction.

By varying the mesh size it was determined that the values of $N_{\theta\phi}$ as presented in table I are in error by no more than 1 unit in the last place retained.

The Displacement v

The displacement v in the ϕ-direction was calculated by the same method as that used to calculate N_θ, a five-point central-difference equation utilizing successive over-relaxation. The difference equation is

$$v^{(n+1)}(\theta,\phi) = \frac{-\omega}{-\frac{2\sin^2\phi}{(\Delta\phi)^2} + 1 - \frac{2}{(\Delta\theta)^2}} \left\{ v^{(n)}(\theta,\phi+\Delta\phi)\left[\frac{\sin^2\phi}{(\Delta\phi)^2} - \frac{\sin\phi\cos\phi}{2\Delta\phi}\right] \right.$$

$$+ v^{(n+1)}(\theta,\phi-\Delta\phi)\left[\frac{\sin^2\phi}{(\Delta\phi)^2} + \frac{\sin\phi\cos\phi}{2\Delta\phi}\right] + \left[v^{(n)}(\theta+\Delta\theta,\phi) + v^{(n+1)}(\theta-\Delta\theta,\phi)\right]\frac{1}{(\Delta\theta)^2}$$

$$\left. - \frac{4r(1+\mu)}{Et} N_\theta(\theta,\phi)\sin\phi\cos\phi \right\} - (\omega - 1)v^{(n)}(\theta,\phi) \qquad \text{(C10)}$$

$$v = 0 \qquad (\theta = 0) \qquad \text{(C11)}$$

$$v = 0 \qquad \left(\theta = \frac{\pi}{2}\right) \qquad \text{(C12)}$$

$$v = 0 \qquad (\phi = 0) \qquad \text{(C13)}$$

$$v = 0 \qquad \left(\phi = \frac{\pi}{2}\right) \qquad \text{(C14)}$$

Because the right-hand side of the partial differential equation for v, equation (35), could be modified in such a way that N_θ is the only unknown (eq. (36)), the mesh size could be made as fine for v as it was for N_θ. For this reason, good accuracy was obtained in the calculation of the displacement v. Thus, the values of v given in table I are correct to one unit in the last digit retained.

The Displacement w

The displacement w normal to the surface of the sphere was calculated from the strain-displacement relation (29). That relation, written in terms of differences and with the stress resultant N_θ replacing the strain, is

$$w = -\frac{r(1-\mu)}{Et} N_\theta - \frac{v(\theta,\phi+\Delta\phi) - v(\theta,\phi-\Delta\phi)}{2\Delta\phi} \qquad \text{(C15)}$$

APPENDIX C

The results of varying the mesh size indicate that w is correct to four places to the right of the decimal point. That number of digits is retained in table I.

The Displacement u

As indicated in the body of the report, rather than calculating the displacement u in the θ-direction, the quantity $\bar{u} = \frac{u}{\sin \phi}$ was calculated. The equation used for the calculation is

$$\frac{\partial \bar{u}}{\partial \phi} = \frac{-\frac{\partial v}{\partial \theta} + \frac{2r(1+\mu)}{Et} N_{\theta\phi} \sin \phi}{\sin^2 \phi} \tag{C16}$$

The behavior of this expression at $\phi = 0$ is determined by expressing the numerator and denominator on the right-hand side of equation (C16) in powers of ϕ. In order to do this it is first necessary to have the series expansions for N_θ, $N_{\theta\phi}$, and v.

Let

$$N_\theta = N_{\theta,0} + N_{\theta,1}\phi + N_{\theta,2}\phi^2 + \cdots \tag{C17}$$

$$N_{\theta\phi} = N_{\theta\phi,0} + N_{\theta\phi,1}\phi + N_{\theta\phi,2}\phi^2 + \cdots \tag{C18}$$

$$v = v_0 + v_1\phi + v_2\phi^2 + \cdots \tag{C19}$$

The second term $N_{\theta,1}$ in the N_θ series is obtained in the same way that $N_{\theta,0}$ was obtained in appendix B – that is, by substituting the series expansion for N_θ into the governing partial differential equation, equation (B1), by setting equal to zero the coefficients of each power of ϕ, and by utilizing boundary conditions which have also been expanded in powers of ϕ. The first two coefficients are

$$N_{\theta,0} = -\frac{3A}{8} \sin 2\theta \tag{C20}$$

$$N_{\theta,1} = -\frac{A}{2} \cos 3\theta \tag{C21}$$

The first two terms in the series expansion for $N_{\theta\phi}$ are obtained in a similar manner. All terms in equation (11) are expanded in powers of ϕ and the equation is assumed to hold for each power of ϕ. By using the results given in equations (C20) and (C21), the quantities $N_{\theta\phi,0}$ and $N_{\theta\phi,1}$ are given by

$$N_{\theta\phi,0} = \frac{3A}{8} \cos 2\theta \tag{C22}$$

$$N_{\theta\phi,1} = -\frac{A}{2} \sin 3\theta \tag{C23}$$

In the same way, by using equation (36),

$$v_0 = 0 \tag{C24}$$

$$v_1 = \frac{3Ar(1 + \mu)}{8Et} \sin 2\theta \tag{C25}$$

$$v_2 = \frac{Ar(1 + \mu)}{4Et}(\cos 3\theta - \cos \theta) \tag{C26}$$

After all pertinent results are substituted into equation (C16) written as

$$\frac{\partial \bar{u}}{\partial \phi} = \frac{\left[-\frac{\partial v_1}{\partial \theta} + \frac{2r(1 + \mu)}{Et} N_{\theta\phi,0}\right]\phi + \left[-\frac{\partial v_2}{\partial \theta} + \frac{2r(1 + \mu)}{Et} N_{\theta\phi,1}\right]\phi^2 + \cdots}{\phi^2 + \cdots} \tag{C27}$$

it is seen that there is no singularity at the pole and

$$\left.\frac{\partial \bar{u}}{\partial \phi}\right|_{\phi=0} = -\frac{rA(1 + \mu)}{4Et}(\sin \theta + \sin 3\theta) \tag{C28}$$

By expanding $\bar{u}$ in powers of ϕ as was done with N_θ, $N_{\theta\phi}$, and v, the distribution of $\bar{u}$ at $\phi = 0$ is determined as

$$\bar{u}(\theta,0) = \frac{3rA}{8Et}(1 + \mu)\cos 2\theta + c \tag{C29}$$

where c is a constant which is affected by a rigid-body rotation. In the present analysis c is set equal to zero.

Because of the small differences that occur in the numerator of equation (C16) for values of ϕ near $\phi = 0$, the value of $\partial\bar{u}/\partial\phi$ adjacent to the pole was calculated with an eight-point interpolation formula utilizing the value of $\partial\bar{u}/\partial\phi$ calculated at the pole and seven other values calculated at points at least two stations away from the pole. Equation (C28) was used to obtain the value of $\partial\bar{u}/\partial\phi$ at the pole, and (C16) was used to calculate $\partial\bar{u}/\partial\phi$ at stations not adjacent to the pole.

With the above information it is possible to solve for $\bar{u}$ by using equation (C16) and a Runge-Kutta method. A contour plot of $\frac{uEt}{rA(1 + \mu)\sin \phi}$ is shown in figure 11 and the values are given in table I.

REFERENCES

1. Cooper, John E.: Application of Inflatable Structures to Station Keeping of Passive Communications Satellites. Second Aerospace Expandable Structures Conference, AFAPL-TR-65-108, U.S. Air Force, 1965, pp. 215-233.

2. Mechtly, E. A.: The International System of Units – Physical Constants and Conversion Factors. NASA SP-7012, 1964.

3. Sears, Francis Weston; and Zemansky, Mark W.: University Physics. Part 2 – Electricity and Magnetism, Optics, and Atomic Physics. Second ed., Addison-Wesley Pub. Co., Inc., c.1955, pp. 570-571.

4. Flügge, Wilhelm: Stresses in Shells. Springer-Verlag (Berlin), 1960.

5. Girkmann, Karl: Flächentragwerke, Springer-Verlag (Vienna), 1959, pp. 379-380.

6. Young, David M., Jr.: The Numerical Solution of Elliptic and Parabolic Partial Differential Equations. Survey of Numerical Analysis, John Todd, ed., McGraw-Hill Book Co., Inc., 1962, pp. 380-438.

7. Milne, William Edmund: Numerical Solution of Differential Equations. John Wiley & Sons, Inc., c.1953, p. 72.

8. Fichter, Wilbur B.; McComb, Harvey G., Jr.; Leonard, Robert W.; and Fralich, Robert W.: Buckling of the Echo A-12 Passive Communications Satellite. NASA TN D-2353, 1964.

TABLE I.- NUMERICAL VALUES OF THE STRESS RESULTANTS AND DISPLACEMENTS

$\left[\phi = \frac{n\pi}{20} \text{ radians}\right]$

n	$\frac{N_\theta}{A}$	$\frac{N_{\theta\phi}}{A}$	$\frac{uEt}{rA(1+\mu)\sin\phi}$	$\frac{vEt}{rA(1+\mu)}$	$\frac{wEt}{rA(1+\mu)}$	$\frac{N_n}{A}$
			$\theta = 0$			
0	0.00000	0.3750	0.375	0.00000	0.0000	0.3750
1	-.07822	.3704	.375	.00000	.0782	.3796
2	-.15451	.3566	.375	.00000	.1545	.3889
3	-.22700	.3341	.375	.00000	.2270	.4040
4	-.29389	.3034	.375	.00000	.2939	.4224
5	-.35355	.2652	.375	.00000	.3536	.4420
6	-.40451	.2204	.375	.00000	.4045	.4607
7	-.44550	.1702	.375	.00000	.4455	.4769
8	-.47553	.1159	.375	.00000	.4755	.4894
9	-.49384	.0587	.375	.00000	.4938	.4973
10	-.50000	.0000	.375	.00000	.5000	.5000
			$\theta = \frac{\pi}{20}$ radians			
0	-0.11589	0.3567	0.357	0.00000	0.0000	0.3750
1	-.18050	.3196	.334	.01734	.0773	.3670
2	-.23465	.2786	.313	.03199	.1526	.3643
3	-.27904	.2377	.294	.04280	.2242	.3666
4	-.31467	.1978	.277	.04905	.2903	.3717
5	-.34261	.1599	.262	.05043	.3492	.3781
6	-.36390	.1242	.250	.04708	.3995	.3845
7	-.37946	.0908	.240	.03946	.4400	.3902
8	-.39003	.0594	.234	.02836	.4696	.3945
9	-.39615	.0293	.230	.01482	.4877	.3972
10	-.39816	.0000	.228	.00000	.4938	.3982
			$\theta = \frac{2\pi}{20}$ radians			
0	-0.22044	0.3034	0.303	0.00000	0.0000	0.3750
1	-.25896	.2433	.263	.03199	.0744	.3554
2	-.28476	.1895	.226	.05741	.1470	.3420
3	-.30121	.1441	.195	.07498	.2159	.3339
4	-.31109	.1068	.168	.08415	.2795	.3289
5	-.31655	.0770	.145	.08503	.3362	.3258
6	-.31922	.0537	.127	.07826	.3847	.3237
7	-.32027	.0356	.113	.06487	.4237	.3222
8	-.32050	.0215	.103	.04627	.4522	.3212
9	-.32044	.0101	.097	.02406	.4696	.3206
10	-.32039	.0000	.095	.00000	.4755	.3204

n	$\frac{N_\theta}{A}$	$\frac{N_{\theta\phi}}{A}$	$\frac{uEt}{rA(1+\mu)\sin\phi}$	$\frac{vEt}{rA(1+\mu)}$	$\frac{wEt}{rA(1+\mu)}$	$\frac{N_n}{A}$
			$\theta = \frac{3\pi}{20}$ radians			
0	-0.30341	0.2204	0.220	0.00000	0.0000	0.3750
1	-.30951	.1517	.169	.04280	.0697	.3447
2	-.30702	.0981	.125	.07498	.1377	.3223
3	-.30005	.0587	.087	.09595	.2022	.3057
4	-.29127	.0309	.056	.10587	.2618	.2929
5	-.28232	.0125	.031	.10552	.3150	.2826
6	-.27421	.0016	.011	.09606	.3604	.2742
7	-.26753	-.0036	-.004	.07898	.3969	.2676
8	-.26259	-.0046	-.014	.05601	.4236	.2626
9	-.25958	-.0030	-.021	.02902	.4400	.2596
10	-.25856	.0000	-.023	.00000	.4454	.2586
			$\theta = \frac{4\pi}{20}$ radians			
0	-0.35667	0.1159	0.116	0.00000	0.0000	0.3750
1	-.33091	.0535	.061	.04905	.0633	.3352
2	-.30500	.0110	.016	.08415	.1250	.3052
3	-.28132	-.0159	-.021	.10587	.1836	.2818
4	-.26088	-.0310	-.051	.11525	.2377	.2627
5	-.24394	-.0373	-.075	.11363	.2860	.2468
6	-.23048	-.0369	-.094	.10258	.3272	.2334
7	-.22029	-.0316	-.109	.08382	.3604	.2225
8	-.21318	-.0229	-.119	.05919	.3847	.2144
9	-.20899	-.0120	-.124	.03059	.3995	.2093
10	-.20760	.0000	-.126	.00000	.4044	.2076
			$\theta = \frac{5\pi}{20}$ radians			
0	-0.37500	0.0000	0.000	0.00000	0.0000	0.3750
1	-.32419	-.0432	-.050	.05044	.0553	.3271
2	-.28273	-.0675	-.090	.08503	.1092	.2907
3	-.24968	-.0786	-.123	.10552	.1605	.2618
4	-.22374	-.0803	-.149	.11363	.2078	.2377
5	-.20369	-.0753	-.171	.11110	.2500	.2172
6	-.18854	-.0654	-.187	.09966	.2860	.1996
7	-.17750	-.0519	-.200	.08106	.3150	.1849
8	-.16999	-.0359	-.209	.05706	.3362	.1737
9	-.16564	-.0184	-.214	.02944	.3491	.1667
10	-.16421	.0000	-.216	.00000	.3535	.1642

TABLE I.- NUMERICAL VALUES OF THE STRESS RESULTANTS AND DISPLACEMENTS – Concluded

$\left[\phi = \frac{n\pi}{20} \text{ radians}\right]$

n	$\frac{N_\theta}{A}$	$\frac{N_{\theta\phi}}{A}$	$\frac{uEt}{rA(1+\mu)\sin\phi}$	$\frac{vEt}{rA(1+\mu)}$	$\frac{wEt}{rA(1+\mu)}$	$\frac{N_n}{A}$
			$\theta = \frac{6\pi}{20}$ radians			
0	-0.35667	-0.1159	-0.116	0.00000	0.0000	0.3750
1	-.29210	-.1317	-.156	.04708	.0459	.3204
2	-.24429	-.1344	-.188	.07826	.0908	.2788
3	-.20879	-.1292	-.214	.09606	.1334	.2455
4	-.18237	-.1184	-.235	.10258	.1727	.2175
5	-.16278	-.1038	-.253	.09966	.2078	.1930
6	-.14842	-.0862	-.266	.08898	.2377	.1716
7	-.13818	-.0664	-.277	.07212	.2618	.1533
8	-.13134	-.0451	-.284	.05064	.2795	.1389
9	-.12741	-.0228	-.288	.02609	.2902	.1294
10	-.12613	.0000	-.290	.00000	.2938	.1261
			$\theta = \frac{7\pi}{20}$ radians			
0	-0.30341	-0.2204	-0.220	0.00000	0.0000	0.3750
1	-.23862	-.2061	-.247	.03946	.0355	.3153
2	-.19347	-.1878	-.270	.06487	.0701	.2696
3	-.16144	-.1679	-.289	.07898	.1030	.2329
4	-.13843	-.1467	-.305	.08382	.1334	.2017
5	-.12181	-.1244	-.319	.08106	.1605	.1741
6	-.10987	-.1010	-.330	.07212	.1836	.1492
7	-.10149	-.0766	-.338	.05831	.2022	.1272
8	-.09595	-.0515	-.344	.04088	.2158	.1089
9	-.09278	-.0259	-.347	.02104	.2242	.0963
10	-.09176	.0000	-.349	.00000	.2270	.0918
			$\theta = \frac{8\pi}{20}$ radians			
0	-0.22044	-0.3034	-0.303	0.00000	0.0000	0.3750
1	-.16853	-.2623	-.318	.02836	.0241	.3118
2	-.13375	-.2265	-.333	.04627	.0477	.2631
3	-.10979	-.1952	-.346	.05601	.0701	.2240
4	-.09297	-.1662	-.357	.05919	.0908	.1905
5	-.08102	-.1383	-.367	.05706	.1092	.1603
6	-.07255	-.1109	-.376	.05064	.1250	.1325
7	-.06667	-.0834	-.382	.04088	.1376	.1068
8	-.06280	-.0558	-.387	.02863	.1469	.0840
9	-.06060	-.0279	-.390	.01472	.1526	.0667
10	-.05989	.0000	-.391	.00000	.1545	.0599

n	$\frac{N_\theta}{A}$	$\frac{N_{\theta\phi}}{A}$	$\frac{uEt}{rA(1+\mu)\sin\phi}$	$\frac{vEt}{rA(1-\mu)}$	$\frac{wEt}{rA(1+\mu)}$	$\frac{N_n}{A}$
			$\theta = \frac{9\pi}{20}$ radians			
0	-0.11589	-0.3567	-0.357	0.00000	0.0000	0.3750
1	-.08712	-.2972	-.363	.01482	.0122	.3097
2	-.06828	-.2500	-.372	.02406	.0241	.2591
3	-.05552	-.2114	-.381	.02902	.0355	.2186
4	-.04667	-.1776	-.389	.03059	.0460	.1837
5	-.04045	-.1464	-.397	.02943	.0553	.1519
6	-.03607	-.1165	-.404	.02609	.0633	.1220
7	-.03304	-.0872	-.409	.02104	.0697	.0933
8	-.03106	-.0581	-.413	.01472	.0744	.0659
9	-.02994	-.0291	-.416	.00757	.0772	.0417
10	-.02957	.0000	-.417	.00000	.0782	.0296
			$\theta = \frac{10\pi}{20}$ radians			
0	0.00000	-0.3750	-0.375	0.00000	0.0000	0.3750
1	.00000	-.3090	-.379	.00000	.0000	.3090
2	.00000	-.2578	-.385	.00000	.0000	.2578
3	.00000	-.2168	-.392	.00000	.0000	.2168
4	.00000	-.1814	-.400	.00000	.0000	.1814
5	.00000	-.1491	-.407	.00000	.0000	.1491
6	.00000	-.1184	-.413	.00000	.0000	.1184
7	.00000	-.0885	-.418	.00000	.0000	.0885
8	.00000	-.0589	-.422	.00000	.0000	.0589
9	.00000	-.0295	-.424	.00000	.0000	.0295
10	.00000	.0000	-.425	.00000	.0000	.0000

"The aeronautical and space activities of the United States shall be conducted so as to contribute . . . to the expansion of human knowledge of phenomena in the atmosphere and space. The Administration shall provide for the widest practicable and appropriate dissemination of information concerning its activities and the results thereof."

—NATIONAL AERONAUTICS AND SPACE ACT OF 1958

NASA SCIENTIFIC AND TECHNICAL PUBLICATIONS

TECHNICAL REPORTS: Scientific and technical information considered important, complete, and a lasting contribution to existing knowledge.

TECHNICAL NOTES: Information less broad in scope but nevertheless of importance as a contribution to existing knowledge.

TECHNICAL MEMORANDUMS: Information receiving limited distribution because of preliminary data, security classification, or other reasons.

CONTRACTOR REPORTS: Scientific and technical information generated under a NASA contract or grant and considered an important contribution to existing knowledge.

TECHNICAL TRANSLATIONS: Information published in a foreign language considered to merit NASA distribution in English.

SPECIAL PUBLICATIONS: Information derived from or of value to NASA activities. Publications include conference proceedings, monographs, data compilations, handbooks, sourcebooks, and special bibliographies.

TECHNOLOGY UTILIZATION PUBLICATIONS: Information on technology used by NASA that may be of particular interest in commercial and other non-aerospace applications. Publications include Tech Briefs, Technology Utilization Reports and Notes, and Technology Surveys.

Details on the availability of these publications may be obtained from:

SCIENTIFIC AND TECHNICAL INFORMATION DIVISION

NATIONAL AERONAUTICS AND SPACE ADMINISTRATION

Washington, D.C. 20546